Probing Crystallinity of Graphene Samples via the Vibrational Density of States

3 AUTHORS, INCLUDING:

Sandeep K. Jain

Utrecht University

2 PUBLICATIONS **1** CITATION

SEE PROFILE

Gerard Barkema

Utrecht University

**185** PUBLICATIONS **4,396** CITATIONS

SEE PROFILE

Probing Crystallinity of Graphene Samples via the Vibrational Density of States

Sandeep K. Jain,[*,†] Vladimir Juričić,[*,†] and Gerard T. Barkema[†,‡]

[†]Institute for Theoretical Physics, Universiteit Utrecht, Leuvenlaan 4, 3584 CE Utrecht, The Netherlands
[‡]Institut-Lorentz, Universiteit Leiden, Niels Bohrweg 2, 2333 CA Leiden, The Netherlands

ABSTRACT: The purity of graphene samples is of crucial importance for their experimental and practical use. In this regard, the detection of the defects is of direct relevance. Here, we show that structural defects in graphene samples give rise to clear signals in the vibrational density of states (VDOS) at specific peaks at high and low frequencies. These can be used as an independent probe of the defect density. In particular, we consider grain boundaries made of pentagon-heptagon pairs, and show that they lead to a shift of the characteristic vibrational D mode toward higher frequency; this distinguishes these line defects from Stone−Wales point defects, which do not lead to such a shift. Our findings may be instrumental for the detection of structural lattice defects using experimental techniques that can directly measure VDOS, such as inelastic electron tunneling and inelastic neutron spectroscopy.
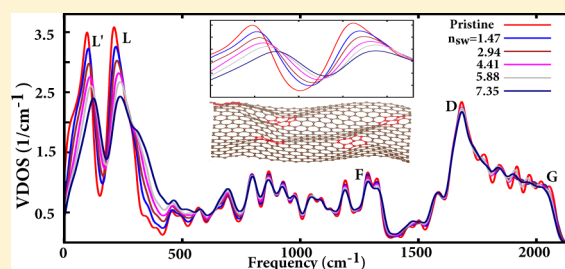
Since it has been experimentally isolated, graphene has attracted enormous attention due to its unusual electronic and mechanical properties.[1] The quality of the crystalline samples is very important for the observation of the hallmark features of graphene, such as ballistic conductivity,[2,3] as well as for its mechanical and chemical properties, e.g., its permeability.[4] Large graphene samples produced, for instance, by chemical vapor-deposition (CVD), exfoliation, or epitaxial growth on metal and SiC substrates are typically polycrystalline and thus contain intrinsic lattice defects, such as grain boundaries,[5−7] dislocations, and Stone−Wales (SW) defects, as well as extrinsic defects, e.g., adatoms.[8] Detection of the lattice defects is of both fundamental and practical relevance, since they are inevitably present in the graphene samples and can significantly alter the graphene's chemical and physical properties.[9] In fact, the defects may not only be detrimental for the properties of graphene, but may also be interesting in their own right, as they may lead to some new effects, not present otherwise,[10−12] and are also important for graphene nano-devices.[13]

Structural defects are especially prominent in this regard.[9] In particular, graphene is a unique two-dimensional crystalline membrane that hosts lattice defects arising due to the flexibility of the carbon atoms in hybridization. As a result, polygons different from hexagons can appear in the lattice structure. Energetically favorable point-like defects of this type include the SW defect obtained when four hexagons are transformed by a bond transposition of 90° into two pentagon-heptagon pairs, thereby conserving the number of the atoms. They can be formed thermally in pristine graphene, but have a formation energy of ~5 eV, and thus pristine graphene may host only a few of them. On the other hand, such defects and similar ones can be frozen in during the annealing process, and it is therefore not surprising that they have been experimentally

observed.[14−16] Moreover, there have been proposals for their controllable production in graphene.[10]

Techniques to characterize the crystal structure of graphene include direct local ones, such as transmission electron microscopy (TEM), scanning tunneling microscopy (STM),[17] and atomic force microscopy (AFM),[18,19] as well as the indirect ones, including Raman spectroscopy,[20−22] X-ray absorption spectroscopy,[23−25] inelastic electron tunneling spectroscopy (IETS),[26−28] and neutron scattering.[29,30] Although widely used, Raman spectroscopy is limited by selection rules to only a certain number of Raman-active vibrational modes, which include the so-called G and 2D peaks located at 1580 and 2680 cm^{-1}, respectively,[31] originating from the G and D phonon modes.[32] In the presence of disorder, due to the breaking of the lattice symmetry, the D mode at 1340 cm^{-1}, Raman inactive in pristine graphene, becomes active. Little is known about the specific experimentally observable signatures of the structural defects, such as point and line defects, in the vibrational spectrum. This is an important problem, especially in light of the recent mapping of the entire vibrational spectrum of graphene by IETS,[33] and reported signature vibrational bands in CVD graphene with defects.[22]

In this Letter, we show that the nature and density of structural point and line defects in graphene samples can be characterized by the specific and distinct features in the vibrational density of states (VDOS). These features are directly detectable in IETS and neutron scattering, which are not limited by selection rules, as opposed to the Raman spectroscopy, and can thus probe the entire vibrational
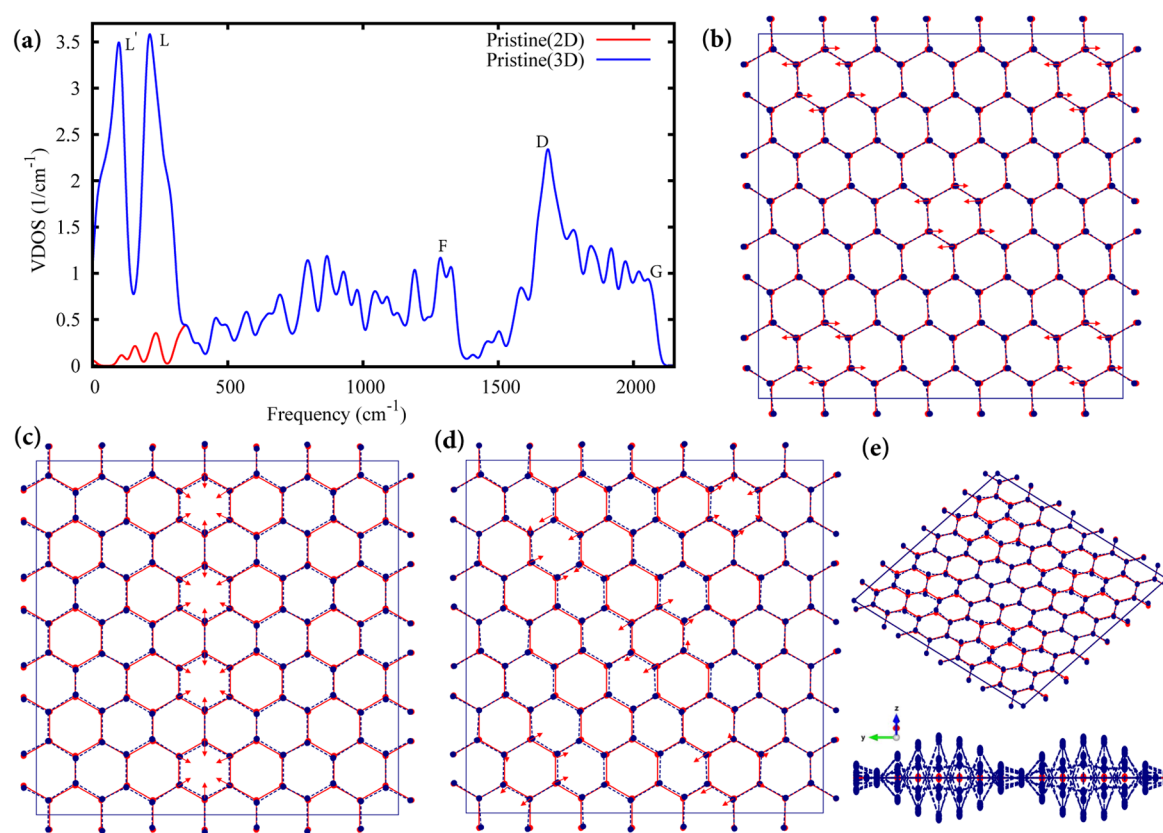
Figure 1. VDOS and the profile of the displacements of the prominent modes in pristine graphene. (a) VDOS of both flat and buckled pristine graphene. (b) Vibrational mode corresponding to Raman active G mode at 2080 cm^{-1}. (c) D mode at 1660 cm^{-1}. (d) F mode at 1280 cm^{-1}. (e) Out-of-plane L mode at 210 cm^{-1}: displacements in the flat graphene's $(x-y)$ plane (top) and in the side $y-z$ plane (bottom).
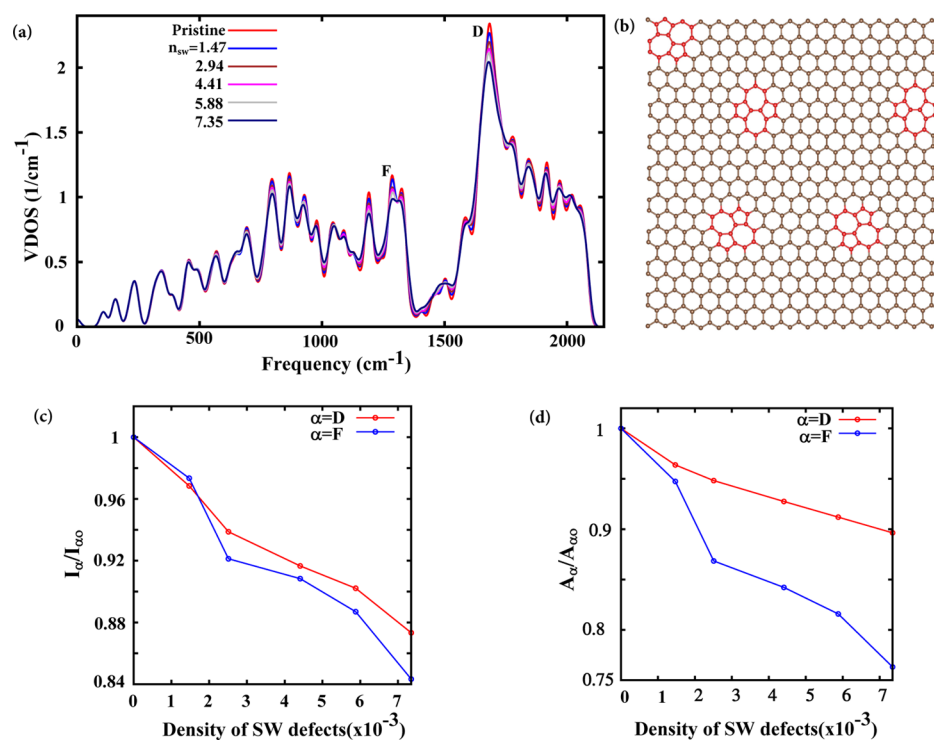

Figure 2. Structure of a flat graphene sample having multiple point SW defects and corresponding VDOS. (a) VDOS of flat graphene samples with different densities of SW defects $n_{SW}(\times 10^{-3})$. (b) The flat graphene sample with five SW defects. (c) Relative decrease in the intensity of D and F peaks at different defect densities. (d) Relative decrease in the number of modes of D and F bands at different defect densities in the range of frequencies in which VDOS is greater than 1.5/cm^{-1} and 1.0/cm^{-1}, respectively.
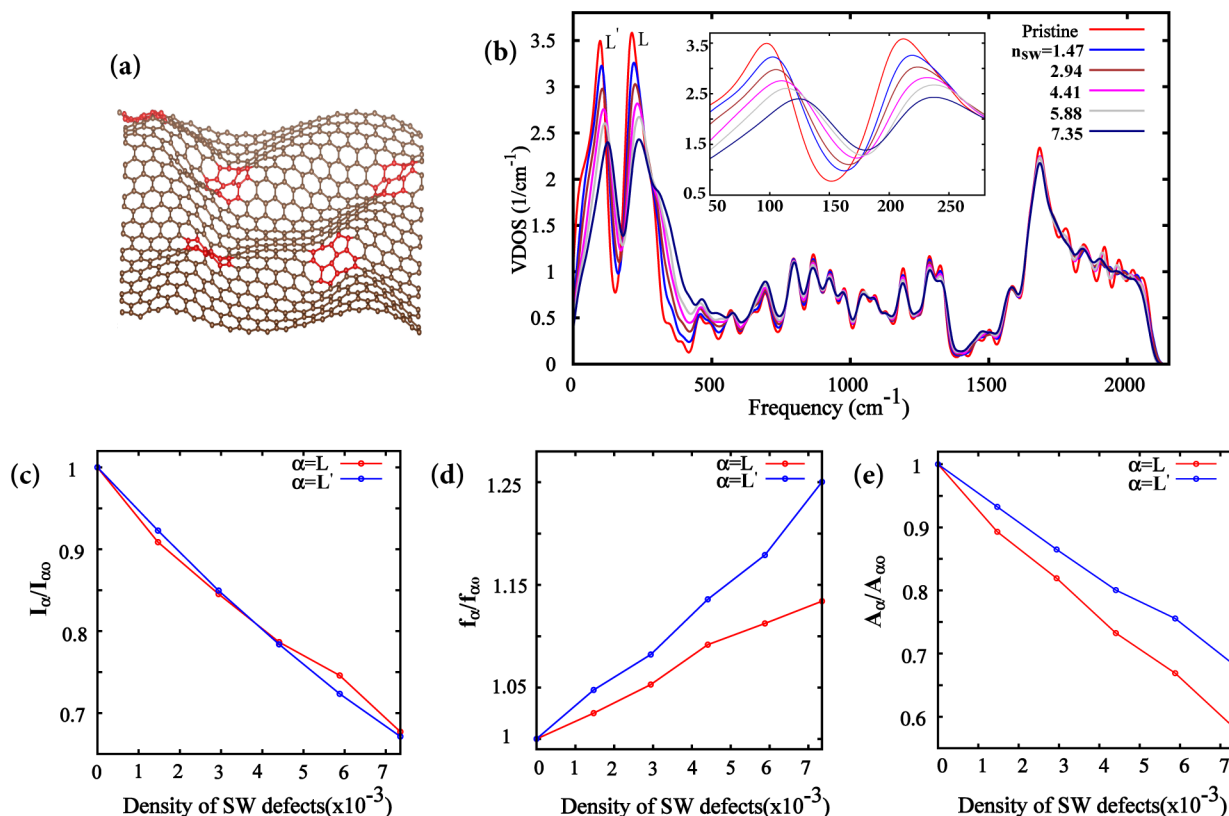
Figure 3. Structure of a buckled graphene sample having multiple point SW defects and corresponding VDOS. (a) The lattice structure of a buckled graphene sample with five SW defects. (b) VDOS of buckled graphene samples with different densities of SW defects $n_{SW}(\times 10^{-3})$. Inset: Low-frequency peaks in VDOS zoomed in. (c) Relative decrease in the intensity of L and L′ modes at different n_{SW}. (d) Relative increase (blue shift) in the frequency of L and L′ modes at different n_{SW}. (e) Relative decrease in the number of modes of L and L′ bands at different defect densities in the range of frequencies in which VDOS is greater than $1.9/cm^{-1}$ and $1.5/cm^{-1}$, respectively.

spectrum.[33] Specifically, using a recently developed effective semiempirical elastic potential,[34] we show that the presence of the point-like SW defects in pristine flat graphene gives rise to a simultaneous decrease in the VDOS of the peaks corresponding to high-frequency D and F modes (Figures 1a and 2a). More importantly, the graphene membrane has a natural tendency to buckle, and as a result, new low-energy vibrational states appear, with particularly pronounced L and L′ peaks (Figure 1a). When the SW defects are introduced, the intensities of these characteristic modes simultaneously decrease, and the peak positions shift toward higher values of frequency (blue shift; see Figure 3b). On the other hand, we find that line defects give rise to a blue shift of the D peak in conjunction with the decrease of its intensity. The substrate plays an important role in the production of graphene samples,[35,36] and we therefore show that the decrease in the VDOS of low-frequency modes without any shift signals its presence.

To calculate the vibrational spectrum of graphene, we use a recently developed effective semiempirical elastic potential[34] given by

$$E = \frac{3}{16}\frac{\alpha}{d^2}\sum_{i,j}(r_{ij}^2 - d^2)^2 + \frac{3}{8}\beta d^2 \sum_{j,i,k}\left(\theta_{jik} - \frac{2\pi}{3}\right)^2 + \gamma\sum_{i,jkl}r_{i,jkl}^2 \tag{1}$$

Here, r_{ij} is the distance between two bonded atoms, θ_{jik} is the angle between the two bonds connecting atom i to atoms j and

k, and $r_{i,jkl}$ is the distance between atom i and the plane through the three atoms j, k, and l connected to atom i. The parameter $\alpha = 26.060$ eV/Å^2 controls bond-stretching and is fitted to the bulk modulus, $\beta = 5.511$ eV/Å^2 controls bond-shearing and is fitted to the shear modulus, $\gamma = 0.517$ eV/Å^2 describes the stability of the graphene sheet against buckling, and $d = 1.420$ Å is the ideal bond length for graphene. The parameters in the potential (eq 1) are obtained by fitting to density-functional theory (DFT) calculations.[34] Additionally, the effect of the substrate to the buckled graphene sample is described by an extra harmonic term

$$E_S = K\sum_i z_i^2 \tag{2}$$

where K is the effective elastic constant for the graphene−substrate interface, and z_i is the distance of atom i from the graphene plane.

The vibrational spectrum is obtained from the above potential. The VDOS represents the number of modes at a certain frequency, and the total area under the VDOS gives the total number of vibrational modes, which is $2N$ for a flat and $3N$ for a buckled graphene sheet, with N being the total number of atoms in the sample. In our plots, the VDOS is convoluted with a Gaussian function with a width of $\sigma = 14$ cm^{-1}, and $N = 680$; this is much larger than system sizes in previous ab initio studies of pristine graphene and graphene with defects.[37−40] Furthermore, we have computed the relative decrease of the number of modes corresponding to the characteristic bands as a function of the defect density. We have

performed this computation by counting the number of modes with a VDOS greater than a certain fixed value selected by the symmetry of the characteristic peak (see Figures 2d and 3e).

Pristine Flat and Buckled Graphene Sheet. We first calculate the VDOS for a flat pristine graphene sample, which serves as the reference spectrum in the following. The plot displayed in Figure 1a shows the characteristic peaks that correspond to D and G vibrational bands, of which only the latter is Raman active.[32] The corresponding modes, shown in Figure 1b,c, transform under E_{2g} and A_{1g} representations of the graphene's D_{6h} point group symmetry, respectively.[41] Notice that the hallmark feature of the monolayer graphene, the Raman-active G mode, which is at the maximum frequency in the vibrational spectrum (see Figure 1a), is positioned at $f_G \simeq 2080$ cm^{-1}, and is therefore offset by about 25% as compared to the experimentally measured value of ~1580 cm^{-1}. The D mode at $f_D \simeq 1660$ cm^{-1} is also shifted by about 25% compared to the experimentally measured 1340 cm^{-1}. Deviations of this magnitude are expected since the parameters of the effective potential are obtained from DFT[34] with similar deviations. However, the form of the displacements of these modes, shown in Figure 1b,c, allows us to identify them as G and D modes, respectively. Furthermore, the vibrational spectrum of graphene features the F mode, shown in Figure 1d, at $f_F \simeq 1280$ cm^{-1}. A flat graphene sheet has a natural tendency to buckle, and this leads to the appearance of additional soft out-of-plane phonon modes in the range of frequencies approximately up to $f_{3D} \sim 300$ cm^{-1}, which is of the order of the energy scale corresponding to the parameter γ describing the buckling in the effective potential 1, $f^\gamma \sim (1/2\pi c)\sqrt{\gamma/m_C} \simeq 150$ cm^{-1}, with $m_C \simeq 2 \times 10^{-26}$ kg as the atomic mass of carbon, and $c = 3 \times 10^8$ m/s the velocity of light. The L and L' modes, the former being a B_{2g} mode (Figure 1e), at frequency $f_L \simeq 210$ cm^{-1} and $f_{L'} \simeq 100$ cm^{-1}, respectively, are especially prominent and, as we show, can be used to probe the point defects in the buckled graphene samples.

Point SW Defects in Flat and Buckled Graphene Samples. We now study the VDOS in flat graphene with point-like SW defects (see Figure 2b). The obtained VDOS is displayed in Figure 2a. We first observe that significant changes in the VDOS occur in the high-frequency region, at frequencies above 500 cm^{-1}. As the density of the defects increases, the VDOS at the peaks decreases. On the other hand, the VDOS at the minima increases, as a consequence of the conservation of the total number of the vibrational modes. Notice in particular that the heights of both D and F peaks simultaneously decrease as more and more defects are added to the sample (see Figure 2c). Particularly, for the highest defect concentration considered, $n_{SW} \simeq 0.7\%$, the VDOS decreases by about 12% and 15% for the D and F modes, respectively. This simultaneous decrease of the two peaks in VDOS represents a hallmark feature of the presence of point defects in the flat graphene sheet, and is certainly experimentally observable. Furthermore, we have found a relative decrease in the number of modes for D and F band of ~10% and ~25%, respectively (see Figure 2d).

The SW defects in the buckled graphene sheet (Figure 3a) have a drastic effect on the low-frequency L and L' vibrational bands. Their presence gives rise to the *simultaneous* decrease of the corresponding peaks in the VDOS, together with the increase of the mode corresponding to the minimum between the two maxima in VDOS, as shown in Figure 3b. The decrease in VDOS of the two peaks is proportional to the defect

concentration (Figure 3c), and it appears to be significant. For instance, for the defect concentration of $n_{SW} \simeq 0.7\%$, it is of the order of 30%. Furthermore, this decrease occurs in conjunction with a systematic blue shift of the maximum of the two modes as the density of the defects increases (see Figure 3d). In particular, for the defect density $n_{SW} \sim 0.7\%$, it is of the order of 25% and 15% for the L' and L modes, respectively. Finally, we find a significant relative decrease in the number of modes as a function of the defect density, which is ~40% and ~30% for the L and L' bands, respectively (see Figure 3e).

Signatures of the Domains and the Substrate in the VDOS. We now turn to the effects of the grain boundary (Figure 4a) to the vibrational modes in flat graphene. As can be seen in Figure 4b, the most prominent features in the VDOS are visible in the high-frequency region. In particular, the intensity of both the F and D bands decreases by approximately 35%, followed by the simultaneous blue shift of both bands by about 2%. These
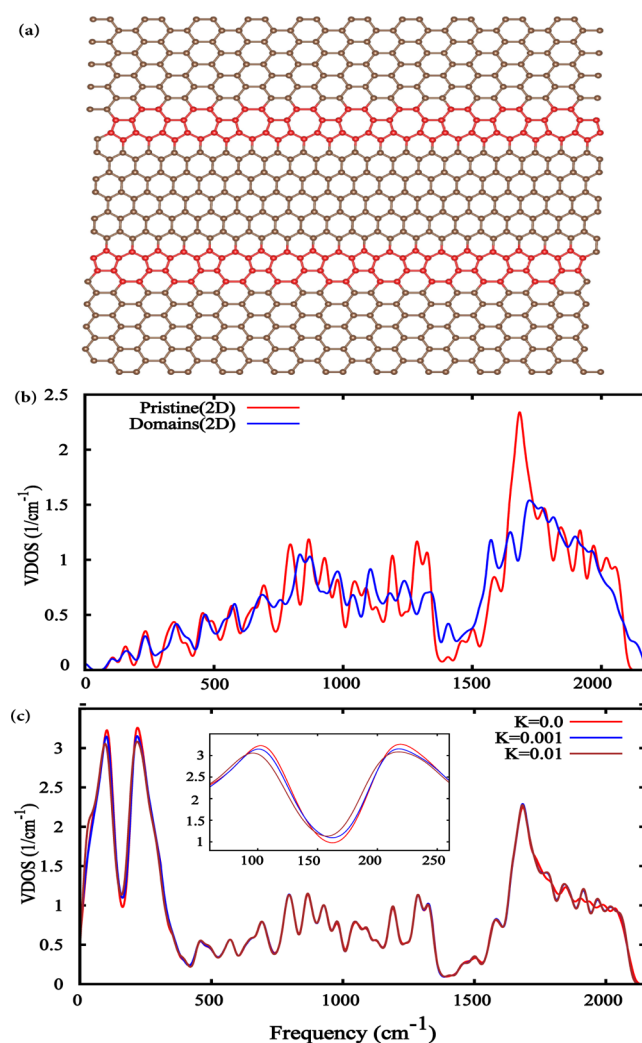

Figure 4. Signature of the line defect and substrate in the VDOS. (a) A graphene sample with two differently oriented domains, with angular mismatch of 30° separated by straight lines of alternating pentagon and heptagon rings. (b) Comparison of the VDOS of pristine graphene and graphene with grain boundaries. (c) VDOS of a graphene sample having one SW defect interfaced by a substrate, with the confining potential given by eq 2, and with the parameter K in eV/Å^2. Inset: Low-frequency part of VDOS with the prominent L and L' peaks.

effects should be contrasted to the behavior of the VDOS in the presence of the point-like SW defects, where no such a shift occurs either in confined two-dimensional geometry or in buckled samples. This blue shift may be attributed to the fact that due to the presence of the defects, the atomic bonds become shorter and therefore stiffer at the position of the defects. The corresponding modes thus become shifted to higher frequencies as compared to the defect-free sample. Notice that this effect is negligible in the case of the confined graphene sample because the relative change of the parameter α in the effective potential (eq 1) is very small (less than 1%). In a buckled sample, on the other hand, due to the fact that the out-of-plane modes are soft, this change is much larger ($\sim$20%) and therefore leads to the obtained more pronounced effect (see the inset of Figure 3b). Finally, we consider the effect of the substrate described by the term (eq 2) in the effective potential. We plot the VDOS for several values of the parameter K in Figure 4c, and observe that the intensity of the low-frequency L and L′ peaks decreases by about 5% (see inset of Figure 4c), without any shift in the position, which is yet different from point defects where such a decrease is followed by the blue shift of the peaks. Notice that this suppression of the intensity of the L and L′ peaks due to the confinement by the substrate is in qualitative agreement with the experimentally observed low-intensity out-of-plane phonon modes in backgated graphene samples placed on a substrate.[33] Although the harmonic confinement potential 2 is certainly a crude description of the real interaction, it may be improved to also accurately capture the quantitative features of the experimentally observed VDOS spectrum.

To conclude, we have shown that the VDOS can be used as a tool to detect the presence of point and line defects in graphene sheets. The confined two-dimensional graphene sample in the presence of the defects shows clear features in the high-frequency VDOS, while the most pronounced effects of the buckling appear at low-frequencies. Given the recent measurement of the entire vibrational spectrum of backgated graphene placed on a substrate using IETS,[33] we hope that our findings will stimulate further experiments to probe the structural defects in this material. Our results can also be used to calculate the corresponding Raman response using different models.[42,43] We would like to point out that our findings may also be applicable to other two-dimensional materials that could be described by a semiempirical potential of the form of eq 1, such as nanoporous carbon.[44,45] We hope that these results will stimulate further studies of vibrational properties of other carbon-based nanomaterials such as carbon-nanotubes,[46,47] graphene nanoribbons,[48] and functionalized graphene.[49]

■ AUTHOR INFORMATION

Corresponding Authors
*E-mail: S.K.Jain@uu.nl.
*E-mail: V.Juricic@uu.nl.

Notes
The authors declare no competing financial interest.

■ ACKNOWLEDGMENTS

■ REFERENCES

(1) Castro Neto, A. H.; Guinea, F.; Peres, N. M. R.; Novoselov, K. S.; Geim, A. K. The Electronic Properties of Graphene. *Rev. Mod. Phys.* **2009**, *81*, 109−162.

(2) Du, X.; Skachko, I.; Barker, A.; Andrei, E. Y. Approaching Ballistic Transport in Suspended Graphene. *Nat. Nanotechnol.* **2008**, *3*, 491−495.

(3) Bolotin, K.; Sikes, K.; Jiang, Z.; Klima, M.; Fudenberg, G.; Hone, J.; Kim, P.; Stormer, H. Ultrahigh Electron Mobility in Suspended Graphene. *Solid State Commun.* **2008**, *146*, 351−355.

(4) Nair, R. R.; Wu, H. A.; Jayaram, P. N.; Grigorieva, I. V.; Geim, A. K. Unimpeded Permeation of Water through Helium-Leak-Tight Graphene-Based Membranes. *Science* **2012**, *335*, 442−444.

(5) Yazyev, O. V.; Chen, Y. P. Polycrystalline Graphene and Other Two-Dimensional Materials. *Nat. Nanotechnol.* **2014**, *9*, 755−767.

(6) Rasool, H. I.; Ophus, C.; Zhang, Z.; Crommie, M. F.; Yakobson, B. I.; Zettl, A. Conserved Atomic Bonding Sequences and Strain Organization of Graphene Grain Boundaries. *Nano Lett.* **2014**, *14*, 7057−7063.

(7) Tison, Y.; Lagoute, J.; Repain, V.; Chacon, C.; Girard, Y.; Joucken, F.; Sporken, R.; Gargiulo, F.; Yazyev, O. V.; Rousset, S. Grain Boundaries in Graphene on SiC(0001) Substrate. *Nano Lett.* **2014**, *14*, 6382−6386.

(8) Araujo, P. T.; Terrones, M.; Dresselhaus, M. S. Defects and Impurities in Graphene-Like Materials. *Mater. Today* **2012**, *15*, 98−109.

(9) Banhart, F.; Kotakoski, J.; Krasheninnikov, A. V. Structural Defects in Graphene. *ACS Nano* **2011**, *5*, 26−41.

(10) Lu, J.; Bao, Y.; Su, C. L.; Loh, K. P. Properties of Strained Structures and Topological Defects in Graphene. *ACS Nano* **2013**, *7*, 8350−8357.

(11) Liu, L.; Qing, M.; Wang, Y.; Chen, S. Defects in Graphene: Generation, Healing, and their Effects on the Properties of Graphene: A Review. *J. Mater. Sci. Technol.* **2015**, *31*, 599−606.

(12) Guryel, S.; Hajgató, B.; Dauphin, Y.; Blairon, J.-M.; Edouard Miltner, H.; De Proft, F.; Geerlings, P.; Van Lier, G. Effect of Structural Defects and Chemical Functionalisation on the Intrinsic Mechanical Properties of Graphene. *Phys. Chem. Chem. Phys.* **2013**, *15*, 659−665.

(13) Vicarelli, L.; Heerema, S. J.; Dekker, C.; Zandbergen, H. W. Controlling Defects in Graphene for Optimizing the Electrical Properties of Graphene Nanodevices. *ACS Nano* **2015**, *9*, 3428−3435.

(14) Hashimoto, A.; Suenaga, K.; Gloter, A.; Urita, K.; Iijima, S. Direct Evidence for Atomic Defects in Graphene Layers. *Nature* **2004**, *430*, 870−873.

(15) Meyer, J. C.; Kisielowski, C.; Erni, R.; Rossell, M. D.; Crommie, M. F.; Zettl, A. Direct Imaging of Lattice Atoms and Topological Defects in Graphene Membranes. *Nano Lett.* **2008**, *8*, 3582−3586.

(16) Kotakoski, J.; Krasheninnikov, A. V.; Kaiser, U.; Meyer, J. C. From Point Defects in Graphene to Two-Dimensional Amorphous Carbon. *Phys. Rev. Lett.* **2011**, *106*, 105505.

(17) Andrei, E. Y.; Li, G.; Du, X. Electronic Properties of Graphene: A Perspective from Scanning Tunneling Microscopy and Magneto-transport. *Rep. Prog. Phys.* **2012**, *75*, 056501.

(18) Boneschanscher, M. P.; Hämäläinen, S. K.; Liljeroth, P.; Swart, I. Sample Corrugation Affects the Apparent Bond Lengths in Atomic Force Microscopy. *ACS Nano* **2014**, *8*, 3006−3014.

(19) Dedkov, Y.; Voloshina, E. Multichannel Scanning Probe Microscopy and Spectroscopy of Graphene Moire Structures. *Phys. Chem. Chem. Phys.* **2014**, *16*, 3894−3908.

(20) Kudin, K. N.; Ozbas, B.; Schniepp, H. C.; Prud'homme, R. K.; Aksay, I. A.; Car, R. Raman Spectra of Graphite Oxide and Functionalized Graphene Sheets. *Nano Lett.* **2008**, *8*, 36−41.

(21) Ferrari, A. C.; Basko, D. M. Raman Spectroscopy as a Versatile Tool for Studying the Properties of Graphene. *Nat. Nanotechnol.* **2013**, *8*, 235−246.

(22) Matz, D. L.; Sojoudi, H.; Graham, S.; Pemberton, J. E. Signature Vibrational Bands for Defects in CVD Single-Layer Graphene by Surface-Enhanced Raman Spectroscopy. *J. Phys. Chem. Lett.* **2015**, *6*, 964−969.

(23) Lee, V.; Park, C.; Jaye, C.; Fischer, D. A.; Yu, Q.; Wu, W.; Liu, Z.; Bao, J.; Pei, S.-S.; Smith, C.; et al. Substrate Hybridization and Rippling of Graphene Evidenced by Near-Edge X-ray Absorption Fine Structure Spectroscopy. *J. Phys. Chem. Lett.* **2010**, *1*, 1247−1253.

(24) De Jesus, L. R.; Dennis, R. V.; Depner, S. W.; Jaye, C.; Fischer, D. A.; Banerjee, S. Inside and Outside: X-ray Absorption Spectroscopy Mapping of Chemical Domains in Graphene Oxide. *J. Phys. Chem. Lett.* **2013**, *4*, 3144−3151.

(25) Mohr, M.; Maultzsch, J.; Dobardzic, E.; Reich, S.; Milosevic, I.; Damnjanovic, M.; Bosak, A.; Krisch, M.; Thomsen, C. Phonon Dispersion of Graphite by Inelastic X-Ray Scattering. *Phys. Rev. B: Condens. Matter Mater. Phys.* **2007**, *76*, 035439.

(26) Vitali, L.; Schneider, M. A.; Kern, K.; Wirtz, L.; Rubio, A. Phonon and Plasmon Excitation in Inelastic Electron Tunneling Spectroscopy of Graphite. *Phys. Rev. B: Condens. Matter Mater. Phys.* **2004**, *69*, 121414(R).

(27) Cervenka, J.; van de Ruit, K.; Flipse, C. F. J. Giant Inelastic Tunneling in Epitaxial Graphene Mediated by Localized States. *Phys. Rev. B: Condens. Matter Mater. Phys.* **2010**, *81*, 205403.

(28) Palsgaard, M. L. N.; Andersen, N. P.; Brandbyge, M. Unravelling the Role of Inelastic Tunneling into Pristine and Defected Graphene. *Phys. Rev. B: Condens. Matter Mater. Phys.* **2015**, *91*, 121403(R).

(29) Rols, S.; Benes, Z.; Anglaret, E.; Sauvajol, J. L.; Papanek, P.; Fischer, J. E.; Coddens, G.; Schober, H.; Dianoux, A. J. Phonon Density of States of Single-Wall Carbon Nanotubes. *Phys. Rev. Lett.* **2000**, *85*, 5222−5225.

(30) Cavallari, C.; Pontiroli, D.; Jiménez-Ruiz, M.; Ivanov, A.; Mazzani, M.; Gaboardi, M.; Aramini, M.; Brunelli, M.; Riccò, M.; Rols, S. Hydrogen on Graphene Investigated by Inelastic Neutron Scattering. *J. Phys.: Conf. Ser.* **2014**, *554*, 012009.

(31) Ferrari, A. C.; Meyer, J. C.; Scardaci, V.; Casiraghi, C.; Lazzeri, M.; Mauri, F.; Piscanec, S.; Jiang, D.; Novoselov, K. S.; Roth, S.; et al. Raman Spectrum of Graphene and Graphene Layers. *Phys. Rev. Lett.* **2006**, *97*, 187401.

(32) Jorio, A.; Dresselhaus, M.; Saito, R.; Dresselhaus, G. *Raman Spectroscopy in Graphene Related Systems*; Willey VCH: Weinheim, Germany, 2011.

(33) Natterer, F. D.; Zhao, Y.; Wyrick, J.; Chan, Y.-H.; Ruan, W.-Y.; Chou, M.-Y.; Watanabe, K.; Taniguchi, T.; Zhitenev, N. B.; Stroscio, J. A. Strong Asymmetric Charge Carrier Dependence in Inelastic Electron Tunneling Spectroscopy of Graphene Phonons. *Phys. Rev. Lett.* **2015**, *114*, 245502.

(34) Jain, S. K.; Barkema, G. T.; Mousseau, N.; Fang, C.-M.; van Huis, M. A. Strong Long-Range Relaxations of Structural Defects in Graphene Simulated Using a New Semiempirical Potential. *J. Phys. Chem. C* **2015**, *119*, 9646−9655.

(35) Wang, Y. y.; Ni, Z. h.; Yu, T.; Shen, Z. X.; Wang, H. m.; Wu, Y. h.; Chen, W.; Shen Wee, A. T. Raman Studies of Monolayer Graphene: The Substrate Effect. *J. Phys. Chem. C* **2008**, *112*, 10637−10640.

(36) Wood, J. D.; Schmucker, S. W.; Lyons, A. S.; Pop, E.; Lyding, J. W. Effects of Polycrystalline Cu Substrate on Graphene Growth by Chemical Vapor Deposition. *Nano Lett.* **2011**, *11*, 4547−4554.

(37) Ma, J.; Alfè, D.; Michaelides, A.; Wang, E. Stone-Wales Defects in Graphene and Other Planar sp2 -Bonded Materials. *Phys. Rev. B: Condens. Matter Mater. Phys.* **2009**, *80*, 033407.

(38) Malola, S.; Hakkinen, H.; Koskinen, P. Comparison of Raman Spectra and Vibrational Density of States Between Graphene Nanoribbons with Different Edges. *Eur. Phys. J. D* **2009**, *52*, 71−74.

(39) Mazzamuto, F.; Saint-Martin, J.; Valentin, A.; Chassat, C.; Dollfus, P. Edge Shape Effect on Vibrational Modes in Graphene Nanoribbons: A Numerical Study. *J. Appl. Phys.* **2011**, *109*, 064516.

(40) Shirodkar, S. N.; Waghmare, U. V. Electronic and Vibrational Signatures of Stone-Wales Defects in Graphene: First-Principles Analysis. *Phys. Rev. B: Condens. Matter Mater. Phys.* **2012**, *86*, 165401.

(41) Mapelli, C.; Castiglioni, C.; Zerbi, G.; Mullen, K. Common Force Field for Graphite and Polycyclic Aromatic Hydrocarbons. *Phys. Rev. B: Condens. Matter Mater. Phys.* **1999**, *60*, 12710−12725.

(42) Rao, A. M.; Richter, E.; Bandow, S.; Chase, B.; Eklund, P. C.; Williams, K. A.; Fang, S.; Subbaswamy, K. R.; Menon, M.; Thess, A.; et al. Diameter-Selective Raman Scattering from Vibrational Modes in Carbon Nanotubes. *Science* **1997**, *275*, 187−191.

(43) Basko, D. M. Theory of Resonant Multiphonon Raman Scattering in Graphene. *Phys. Rev. B: Condens. Matter Mater. Phys.* **2008**, *78*, 125418.

(44) Bourgeois, L. N.; Bursill, L. A. High-Resolution Transmission Electron Microscopic Study of Nanoporous Carbon Consisting of Curved Single Graphitic Sheets. *Philos. Mag. A* **1997**, *76*, 753−768.

(45) Smith, M. A.; Foley, H. C.; Lobo, R. F. A Simple Model Describes the PDF of a Non-Graphitizing Carbon. *Carbon* **2004**, *42*, 2041−2048.

(46) Pekker, A.; Botos, A.; Rusznyak, A.; Koltai, J.; Kurti, J.; Kamaras, K. Vibrational Signatures in the Infrared Spectra of Single- and Double-Walled Carbon Nanotubes and their Diameter Dependence. *J. Phys. Chem. Lett.* **2011**, *2*, 2079−2082.

(47) Xin, M.; Wang, F.; Meng, Y.; Tian, C.; Jin, M.; Wang, Z.; Zhang, R. Characteristic Vibrational Modes and Electronic Structures of Carbon Nanotubes Containing Defects. *J. Phys. Chem. C* **2012**, *116*, 292−297.

(48) OuYang, F.; Huang, B.; Li, Z.; Xiao, J.; Wang, H.; Xu, H. Chemical Functionalization of Graphene Nanoribbons by Carboxyl Groups on Stone-Wales Defects. *J. Phys. Chem. C* **2008**, *112*, 12003−12007.

(49) Mattson, E. C.; Johns, J. E.; Pande, K.; Bosch, R. A.; Cui, S.; Gajdardziska-Josifovska, M.; Weinert, M.; Chen, J. H.; Hersam, M. C.; Hirschmugl, C. J. Vibrational Excitations and Low-Energy Electronic Structure of Epoxide-Decorated Graphene. *J. Phys. Chem. Lett.* **2014**, *5*, 212−219.